Research Article

Chao-Chung Peng*, Min-Che Tsai, and Tsai-Ying Chen

Nonlinearity modeling for online estimation of industrial cooling fan speed subject to model uncertainties and state-dependent measurement noise

Abstract: This article presents an online speed estimation method for cooling fans in resource-limited systems, considering modeling uncertainties and measurement noise. In the current thriving information technology era, monitoring the state of cooling fans is crucial, particularly for high-performance artificial intelligence server cabinets. Accurate fan speed estimation can be used not only to detect fan abnormalities but also for speed control-related applications. Several challenges arise in developing speed estimation algorithms, including state-dependent measurement noise variance, errors in nonlinear fan dynamic modeling, and uncertainties in parameter estimation. To address these issues, this study employs the unscented Kalman filter (UKF) algorithm, incorporating state-dependent noise modeling and mathematical modeling of parameter uncertainties. An UKF-based parameter update mechanism is developed to compensate for model uncertainties and estimation errors, improving the speed estimation accuracy. Simulation results indicate that the root-mean-square errors are reduced from 1.3393 with the traditional UKF to 0.7485 with the parameter update mechanism. Experimental verifications further validate the effectiveness of the proposed methods and strategies in addressing the challenges associated with speed estimation in cooling fans under uncertainties and noise interference.

Keywords: cooling fan, speed estimation, model uncertainties, measurement noise, unscented Kalman filter

* **Corresponding author: Chao-Chung Peng,** Department of Aeronautics and Astronautics, National Cheng Kung University, Tainan, Taiwan, e-mail: ccpeng@mail.ncku.edu.tw
Min-Che Tsai, Tsai-Ying Chen: Department of Aeronautics and Astronautics, National Cheng Kung University, Tainan, Taiwan

1 Introduction

In this era of artificial intelligence and technological advancement, the density of high-performance servers and information technology-related equipment is constantly increasing, placing critical stability demands on these devices. The uninterrupted cooling requirements for servers have become a focal point of attention, leading to a sharp increase in the demand for stable, high-performance cooling fans [1,2].

The cooling fan system, composed of a motor and several rotor blades, represents a popular configuration in cooling systems [3]. The utilization of cooling fans not only optimizes the cost in the development phase but also significantly enhances the heat dissipation efficiency. Therefore, it is often regarded as the primary solution for ambient temperature control [4,5].

In the industrial field, cooling fans are widely employed as heat-dissipation devices for equipment such as computers [6], vehicles [7], and server electronics [8]. Cooling fan systems often require extended operational periods; however, prolonged operation may result in system failures. The primary causes of fan system failures often stem from losses or defects in both electrical and mechanical components, or defects in the manufacturing process [9,10].

These failures in cooling fans could result in equipment overheating or more severe damage, consequently causing server shutdowns and data loss. In light of this, the integration of real-time health monitoring and anomaly detection technologies for fans has become an indispensable component of modern industrial operations [11,12]. It provides an intelligent and proactive approach, ensuring the continuous and efficient operation of fans in critical applications. This approach thereby offers robust support for system stability and reliability.

Recent studies have proposed methodologies for dynamic modeling of cooling fan systems, parameter identification, and online monitoring of fan speeds [13,14]. This is achieved by

establishing a virtual fan system, enabling sensor-less online monitoring of fans.

To achieve precise monitoring of fan operations, the measurement of the fan's state and subsequent data processing are crucial [15,16]. However, this measurement process is often accompanied by noise interference, leading to uncertainties in fan monitoring. These uncertainties result in reduced accuracy, increased risk of false alarms, negative impacts on diagnosis and prediction, and greater complexity in data processing. Therefore, obtaining a clean state signal in real time despite measurement noise is a crucial technological challenge in nonlinear cooling fan systems.

Estimating the internal state of dynamic systems based on a set of noisy observational data has been a significant challenge encountered across diverse fields. For linear systems with known Gaussian white noise, Kalman filter (KF) offers the optimal solution for state estimation mean square error [17]. However, real-world dynamic systems are almost invariably nonlinear, which poses a significant challenge. Nonlinear filters can be broadly categorized into two types [18]. The first type involves linearizing the process and observation models around the previous estimate, treating this preceding estimate as the true state. This approach is exemplified by the extended Kalman filter (EKF) model [19,20]. As indicated in previous research papers [21,22], the EKF can be regarded as providing a first-order approximation, thereby offering suboptimal estimates that may lead to state divergence in certain circumstances. Another type of nonlinear filter employs a set of samples to approximate the distribution of the state. Particle filter is a sequential Monte Carlo algorithm that propagates weighted random particles through a nonlinear system and resamples them based on the likelihood weights of the particles [23,24].

Utilizing a greater number of particles can yield higher precision; however, the computational expenses increase. Additionally, Julier *et al.* introduced the unscented Kalman filter (UKF) in which they employed the unscented transform (UT). This method involves the propagation of several sigma points through nonlinear functions, reconstructing the Gaussian distribution foundation for a more accurate estimation of nonlinear system behavior [25,26]. Considering the impact of outliers in polluted distributions and the influence of time-varying noise, the performance of the classical UKF significantly deteriorates. Recent research [27] has proposed an adaptive and robust UKF approach using Gaussian process regression-assisted Variational Bayesian to enhance the traditional UKF estimation performance. Zhu and Fu, by integrating UKF with the improved unscented PF algorithm, enhanced the accuracy of assessing the state of health for lithium-ion batteries [28].

Research related to cooling fans has been explored in previous studies [3,13,14]. However, these studies did not deeply address the issues of online fan speed estimation in the presence of both noise and model uncertainties. Additionally, the model parameters of the fan systems in these studies were considered constant. In real-world scenarios, the model uncertainties may not be exactly known, and the associated fans may vary slowly due to changes from long-term use in the environment and operating conditions. Acquiring accurate fan speed is crucial in the process of implementing speed control and online diagnosis.

It is worth noting that recent studies have demonstrated the feasibility of KF techniques in various fan applications, including speed estimation [29], precise control [30], and fault detection [31]. However, there is still a lack of research specifically focused on online speed estimation for nonlinear industrial cooling fans. Therefore, this work aims to develop a framework for accurate online speed estimation of industrial cooling fans, addressing the issues of noise and model uncertainties.

This study utilizes UKF estimation techniques to conduct a detailed case study on online speed estimation for cooling fan systems. We proposed specialized design and improvement strategies for UKF in fan speed estimation to address the fast dynamics and parameter uncertainties often overlooked in previous research [13]. The objective is to achieve real-time state estimation of the fan speed, tackling challenges arising from measurement noise with state-dependent variance, errors in fan nonlinear dynamic modeling, and uncertainties in parameter estimation. The experimental results demonstrate the practical value of the proposed methods in engineering applications.

The specific contributions of this article include: (1) comparative analysis of model derivation and dynamic behavior of cooling fan systems, (2) comparison between nonlinear model speed estimation *via* EKF and UKF, respectively, (3) analysis and modeling of fan speed measurement noise distribution characteristics, and (4) establishment of a parameter update mechanism under the UKF framework to compensate for parameter estimation errors and model uncertainties, which involves a detailed examination of the dynamic model of cooling fans and provides strategies for setting $\mathbf{Q}$ and $\mathbf{R}$ in fan speed estimation. Finally, (5) validation of the proposed methods through both simulation and experimental cross-verification, confirming the effectiveness of real-time fan speed estimation in the presence of measurement noise. Concisely, the proposed method is scientifically valid and technically sound.

The remaining sections of this article are organized as follows: In Section 2, a comprehensive introduction to the cooling fan system is provided, accompanied by a complete

derivation of the dynamic model. In Section 3, two nonlinear state estimation methods are reviewed, including an introduction to the EKF and UKF (an analysis of their advantages and disadvantages is presented). Section 4 delves into a case study and numerical simulations of cooling fan speed estimation. This includes noise modeling, a review of fan dynamic models, and an exploration of time-varying parameter uncertainties. Based on these conditions, a parameter update mechanism based on UKF is proposed to enhance the accuracy of online fan speed estimation. The implementation of the proposed method is demonstrated on an experimental platform in Section 5, and the accuracy of speed estimation is compared between the traditional UKF and the proposed UKF with a parameter update mechanism. Experimental results confirm the effectiveness of the proposed method. Finally, Section 6 provides the conclusion of the study.

2 Model description of motor-driven cooling fan

A general industrial cooling fan system consists of a driving circuit, a mechanical rotary structure, and a blade. Suppose that the driving system can be simplified as a DC motor, then the overall system can be briefly illustrated in Figure 1, which contains an electrical driving part, a mechanical rotary part, and an external load part.

The governing equation of the electrical driving circuit and the motor mechanism is described as

$$L\frac{\mathrm{d}i(t)}{\mathrm{d}t} + Ri(t) + V_{\mathrm{b}}(t) = V_{\mathrm{in}}(t), \tag{1}$$

where L refers to the inductance, R stands for the resistance, $i(t)$ is the driving current, and $V_{\mathrm{in}}(t)$ represents the applied input voltage. $V_{\mathrm{b}}(t)$ symbolizes the back emf voltage, proportional to the angular velocity $\omega(t)$ of the rotor in the motor, given as $V_{\mathrm{b}}(t) = K_{\mathrm{e}}\omega(t)$, of the back electromotive force (emf) constant K_{e}.
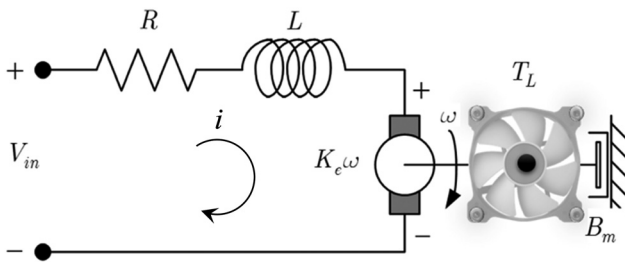

Figure 1: Industrial cooling fan driving system [13].

The motor mechanism can be expressed as

$$J_{\mathrm{m}}\frac{\mathrm{d}\omega(t)}{\mathrm{d}t} + B_{\mathrm{m}}\omega(t) = T_{\mathrm{m}}(t) - T_{\mathrm{L}}(t), \tag{2}$$

in which J_{m} is the rotor motor inertia, B_{m} is the frictional coefficient, and T_{L} is the external load. The motor generates a torque $T_{\mathrm{m}}(t)$ proportional to the armature current, which is $T_{\mathrm{m}}(t) = K_{\mathrm{t}}i(t)$, where K_{t} is the torque constant. Based on the property that the electric power is equivalent to mechanical power, one has

$$(K_e\omega) \cdot i = (K_t i) \cdot \omega, \tag{3}$$

where the left-hand side and the right-hand side represent the electric power and mechanical power, respectively. Based on Eq. (3), it reveals that $K_{\mathrm{e}} = K_{\mathrm{t}} \coloneqq K$.

Since the mechanical dynamics is much slower than the electrical dynamics, the transient response of the electrical circuit can be ignored. As a result,

$$V_{\mathrm{in}} \approx iR + K_e\omega. \tag{4}$$

Based on Eqs. (1)–(3), the system can be simplified to

$$J_{\mathrm{m}}\frac{\mathrm{d}\omega}{\mathrm{d}t} = \frac{K}{R}V_{\mathrm{in}} - \left(\frac{K^2}{R} + B_{\mathrm{m}}\right)\omega - T_{\mathrm{L}}. \tag{5}$$

According to the fan blade aerodynamics in the study of Peng and Li [3], the external load mainly contributes to the drag force induced by the cooling fan. Therefore, T_{L} can be modeled by

$$T_{\mathrm{L}} = C_{\mathrm{d}}\omega^2, \tag{6}$$

where C_{d} refers to the lumped aerodynamic drag coefficient. Substituting Eq. (6) into Eq. (5) and assuming $\tau = V_{\mathrm{in}}$, one can obtain the following equivalent system representation for the cooling fan dynamics [14]:

$$J\dot{\omega}(t) + \alpha\omega(t) + C_D\omega^2(t) = \tau(t), \tag{7}$$

in which the equivalent coefficients are defined as follows:

$$J = J_{\mathrm{m}}\frac{R}{K}, \quad \alpha = K + \frac{R}{K}B_{\mathrm{m}}, \quad C_D = \frac{R}{K}C_{\mathrm{d}}, \tag{8}$$

Eq. (7) represents the complete cooling fan dynamics, where τ stands for the applied torque generated by the pulse width modulator (PWM), J is the lumped moment of inertia, and α refers to the lumped viscosity coefficient.

For simplicity, rewrite Eq. (7) as

$$\dot{\omega}(t) = -a\omega(t) - a_N\omega^2(t) + b\tau(t), \tag{9}$$

in which the equivalent parameters are denoted as

$$a = \frac{\alpha}{J}, \quad a_N = \frac{C_D}{J}, \quad b = \frac{1}{J}. \tag{10}$$

Therefore, the physical model of the cooling fan driving system can be described by a nonlinear state equation.

Based on the known physical model of the cooling fan driving system, relevant literature [13] has proposed a recursive low-pass filtering method for parameter identification. This method can accurately estimate the physical model parameters represented by Eq. (10) in real-time.

In the following section, the reduced order model Eq. (9) will be taken as the plant for online speed estimator development. Based on the modeling described in this section, it can be observed that the system involves parameter-dependent as well as parameter-independent model uncertainties. Therefore, the purpose of this article is to estimate the fan speed online in the presence of these modeling errors and measurement noise.

3 Review of Kalman filtering for nonlinear systems

In the process of modeling the cooling fan system, it becomes evident that the physical model of the fan exhibits nonlinear dynamic characteristics. To address the challenges posed by this nonlinearity, this section introduces two commonly used techniques for nonlinear estimation: the EKF and the UT presented with the UKF. Subsequently, a comparative study between the EKF and UKF is presented. To address the problem of the biased estimates resulting from the model uncertainties appear in both the EKF and UKF, a state estimate refinement strategy of UKF is proposed to generate high precision speed estimates.

3.1 EKF

The EKF is a commonly used technique for estimating the state of a nonlinear dynamic system [20]. It extends the traditional KF to handle nonlinearity by linearizing the system dynamics with the Taylor series expansion.

Consider a nonlinear stochastic process model defined by a state transition model and an observation model

$$\mathbf{x}_k = \mathbf{f}(\mathbf{x}_{k-1}, \mathbf{u}_k) + \mathbf{w}_k, \mathbf{z}_k = \mathbf{h}(\mathbf{x}_k) + \mathbf{v}_k, \qquad (11)$$

where $\mathbf{x}_k \in \mathbb{R}^n$ represents the state vector at time step k and $\mathbf{u}_k \in \mathbb{R}^m$ is the system input. Here, $\mathbf{f}(\cdot) \in \mathbb{R}^n$ and $\mathbf{h}(\cdot) \in \mathbb{R}^l$ represent the nonlinear transition and measurement functions, respectively. The process and measurement noise $\mathbf{w}_k \in \mathbb{R}^n$ and $\mathbf{v}_k \in \mathbb{R}^l$ are also assumed to be independent of each other, with zero-mean Gaussian distributions:

$$\mathcal{P}(\mathbf{w}_k) \sim \mathcal{N}(0, \mathbf{Q}_k), \quad \mathcal{P}(\mathbf{v}_k) \sim \mathcal{N}(0, \mathbf{R}_k), \qquad (12)$$

where $\mathbf{Q}_k$ and $\mathbf{R}_k$ are covariance matrices signifying system model uncertainty and observation model measurement noise, respectively. The zero-mean Gaussian distribution assumptions are valid in this research topic based on the prior work [14].

In the EKF, these nonlinear functions are approximated through linearization around the current state estimate, enabling the application of KF principles. The EKF algorithm can be summarized as follows:

Algorithm 1 EKF

Time update (prediction):
1: $\hat{\mathbf{x}}_k^- \approx \mathbf{f}(\hat{\mathbf{x}}_{k-1}, \mathbf{u}_k)$
2: $\mathbf{P}_k^- = \mathbf{F}_k \mathbf{P}_{k-1} \mathbf{F}_k^T + \mathbf{Q}_k$
Measurement update (correction):
3: $\mathbf{K}_k = \mathbf{P}_k^- \mathbf{H}_k^T (\mathbf{H}_k \mathbf{P}_k^- \mathbf{H}_k^T + \mathbf{R}_k)^{-1}$
4: $\hat{\mathbf{x}}_k = \hat{\mathbf{x}}_k^- + \mathbf{K}_k [\mathbf{z}_k - \mathbf{h}(\hat{\mathbf{x}}_k^-)]$
5: $\mathbf{P}_k = (\mathbf{I} - \mathbf{K}_k \mathbf{H}_k) \mathbf{P}_k^-$

---

where $\mathbf{F}_k$ and $\mathbf{H}_k$ are the Jacobian matrices defined as

$$\mathbf{F}_k = \frac{\partial \mathbf{f}(\hat{\mathbf{x}}_{k-1})}{\partial \mathbf{x}}, \quad \mathbf{H}_k = \frac{\partial \mathbf{h}(\hat{\mathbf{x}}_k^-)}{\partial \mathbf{x}}. \qquad (13)$$

In the prediction step, the algorithm estimates the next state $\hat{\mathbf{x}}_k$ and updates the associated uncertainty $\mathbf{P}_k$ using the nonlinear transition function $\mathbf{f}(\cdot)$. The correction step refines the prediction by assimilating measurement information $\mathbf{z}_k$, adjusting the state estimate based on the Kalman gain $\mathbf{K}_k$, and refining the uncertainty estimate. This EKF algorithm provides a systematic approach to handling nonlinearities, extending the KF's utility in estimating states for dynamic systems.

The EKF utilizes Taylor series expansion to approximate the KF, replacing system matrices with Jacobians. Notably, the EKF is suitable for differentiable models, as it relies on the existence of Jacobians. However, this approach is limited, as it may not work well with non-differentiable or highly nonlinear models, where Jacobians are hard to compute or involve high computational costs. In such cases, linearization may result in larger errors in mean and covariance, potentially leading to divergence of estimates. To better address these issues, UT and UKF will be introduced in the following section.

3.2 UKF

For state estimation of nonlinear models, EKF merely uses one single point to approximate the Gaussian distribution.

If the function is highly nonlinear in this local region, linearization may lead to poor estimates. The UKF handles this problem with UT, which uses a set of sample points to describe the Gaussian model and propagates them through the nonlinear system [26].

To utilize the UKF, the weights of the sigma points need to be determined in advance. For every new-coming measurement $\mathbf{z}_k$, based on the given control input $\mathbf{u}_k$ and the previous state $\hat{\mathbf{x}}_{k-1}$ and covariance $\mathbf{P}_{k-1}$, the sigma points are then generated. Next, similar to the KF and the EKF algorithms, the UKF has prediction and correction steps. In the prediction step, the sigma points are propagated through the transition model.

$$\mathbf{x}_k^{(i)} = \mathbf{f}(\mathbf{x}_{k-1}^{(i)}, \mathbf{u}_k), \tag{14}$$

and the predicted mean (or the prior estimate of state) $\hat{\mathbf{x}}_k^-$ and covariance $\mathbf{P}_k^-$ can be calculated by the propagated sigma points with their weights

$$\hat{\mathbf{x}}_k^- = \sum_{i=0}^{2n} w_m^{(i)} \mathbf{x}_k^{(i)}, \mathbf{P}_k^- = \sum_{i=0}^{2n} w_c^{(i)} (\mathbf{x}_k^{(i)} - \hat{\mathbf{x}}_k^-)(\mathbf{x}_k^{(i)} - \hat{\mathbf{x}}_k^-)^T + \mathbf{Q}_k. \tag{15}$$

In the correction step, the sigma points are transformed through the observation model,

$$\mathbf{Z}_k^{(i)} = \mathbf{h}(\mathbf{x}_k^{(i)}), \tag{16}$$

then the predicted measurement mean and covariance can be calculated as

$$\hat{\mathbf{z}}_k^- = \sum_{i=0}^{2n} w_m^{(i)} \mathbf{Z}_k^{(i)},$$
$$\mathbf{P}_{z,k} = \sum_{i=0}^{2n} w_c^{(i)} (\mathbf{Z}_k^{(i)} - \hat{\mathbf{z}}_k^-)(\mathbf{Z}_k^{(i)} - \hat{\mathbf{z}}_k^-)^T + \mathbf{R}_k. \tag{17}$$

Note that the predicted covariance Eq. (15) and predicted measurement covariance Eq. (17) are made up of the uncertainty of the UT and the process noise $\mathbf{Q}_k$ and measurement noise $\mathbf{R}_k$, respectively.

The cross-covariance matrix between the state space and measurement space is given as

$$\mathbf{P}_{xz,k} = \sum_{i=0}^{2n} w_c^{(i)} (\mathbf{x}_k^{(i)} - \hat{\mathbf{x}}_k^-)(\mathbf{Z}_k^{(i)} - \hat{\mathbf{z}}_k^-)^T. \tag{18}$$

Based on the definition of the error covariance matrix, $\mathbf{P}_{z,k}$ can be expressed as

$$\mathbf{P}_{z,k} = E[(\mathbf{z}_k - \hat{\mathbf{z}}_k^-)(\mathbf{z}_k - \hat{\mathbf{z}}_k^-)^T] = \mathbf{H}_k \mathbf{P}_k^- \mathbf{H}_k^T + \mathbf{R}_k. \tag{19}$$

Similarly, $\mathbf{P}_{xz,k}$ can be written as

$$\mathbf{P}_{xz,k} = E[(\mathbf{x}_k - \hat{\mathbf{x}}_k^-)(\mathbf{z}_k - \hat{\mathbf{z}}_k^-)^T] = \mathbf{P}_k^- \mathbf{H}_k^T. \tag{20}$$

Recalling the Kalman gain in EKF,

$$\mathbf{K}_k = \mathbf{P}_k^- \mathbf{H}_k^T (\mathbf{H}_k \mathbf{P}_k^- \mathbf{H}_k^T + \mathbf{R}_k)^{-1}, \tag{21}$$

one can find out that Eqs. (19) and (20) compose the elements in Eq. (21), therefore yielding the Kalman gain as

$$\mathbf{K}_k = \mathbf{P}_{xz,k} \mathbf{P}_{z,k}^{-1}. \tag{22}$$

The state update equation is given as

$$\hat{\mathbf{x}}_k = \hat{\mathbf{x}}_k^- + \mathbf{K}_k(\mathbf{z}_k - \hat{\mathbf{z}}_k^-). \tag{23}$$

Substituting Eqs. (20) and (22) into the covariance matrix update in EKF gives the covariance matrix update of UKF

$$\mathbf{P}_k = (\mathbf{I} - \mathbf{K}_k \mathbf{H}_k)\mathbf{P}_k^- = \mathbf{P}_k^- - \mathbf{K}_k \mathbf{P}_{z,k} \mathbf{K}_k^T. \tag{24}$$

The algorithm of the UKF is summarized as the pseudocode in Algorithm 2.

Algorithm 2 UKF

Initialize:
1: Determine the initial conditions for the state $\hat{\mathbf{x}}_0 \in \mathbb{R}^n$ and covariance $\mathbf{P}_0 \in \mathbb{R}^{n \times n}$.
2: Set the parameters for generation of sigma points γ, α, and β.
3: Set the weights of sigma points
$$w_m^{(0)} \leftarrow \frac{\gamma}{n+\gamma}, w_c^{(0)} \leftarrow \frac{\gamma}{n+\gamma} + (1 - \alpha^2 + \beta)$$
$$w_m^{(i)}, w_c^{(i)} \leftarrow \frac{1}{2(n+\gamma)}, i = 1, \cdots, 2n$$

Input: New-coming measurement $\mathbf{z}_k$, control $\mathbf{u}_k$, $\hat{\mathbf{x}}_{k-1}$ and $\mathbf{P}_{k-1}$ from the previous recursion.
Output: $\hat{\mathbf{x}}_k$, $\mathbf{P}_k$
Begin interrupt routine
    Sigma Point Generation:
4: $\mathbf{x}_{k-1}^{(i)} = [\hat{\mathbf{x}}_{k-1} \quad \hat{\mathbf{x}}_{k-1} \pm (\sqrt{(n+\gamma)\mathbf{P}_{k-1}})_i]$
    Time update (prediction):
5: $\mathbf{x}_k^{(i)} = \mathbf{f}(\mathbf{x}_{k-1}^{(i)}, \mathbf{u}_k)$
6: $\hat{\mathbf{x}}_k^- = \sum_{i=0}^{2n} w_m^{(i)} \mathbf{x}_k^{(i)}$
7: $\mathbf{P}_k^- = \sum_{i=0}^{2n} w_c^{(i)} (\mathbf{x}_k^{(i)} - \hat{\mathbf{x}}_k^-)(\mathbf{x}_k^{(i)} - \hat{\mathbf{x}}_k^-)^T + \mathbf{Q}_k$
    Measurement update (correction):
8: $\mathbf{Z}_k^{(i)} = \mathbf{h}(\mathbf{x}_k^{(i)})$
9: $\hat{\mathbf{z}}_k^- = \sum_{i=0}^{2n} w_m^{(i)} \mathbf{Z}_k^{(i)}$
10: $\mathbf{P}_{z,k} = \sum_{i=0}^{2n} w_c^{(i)} (\mathbf{Z}_k^{(i)} - \hat{\mathbf{z}}_k^-)(\mathbf{Z}_k^{(i)} - \hat{\mathbf{z}}_k^-)^T + \mathbf{R}_k$
11: $\mathbf{P}_{xz,k} = \sum_{i=0}^{2n} w_c^{(i)} (\mathbf{x}_k^{(i)} - \hat{\mathbf{x}}_k^-)(\mathbf{Z}_k^{(i)} - \hat{\mathbf{z}}_k^-)^T$
12: $\mathbf{K}_k = \mathbf{P}_{xz,k} \mathbf{P}_{z,k}^{-1}$
13: $\hat{\mathbf{x}}_k = \hat{\mathbf{x}}_k^- + \mathbf{K}_k(\mathbf{z}_k - \hat{\mathbf{z}}_k^-)$
14: $\mathbf{P}_k = \mathbf{P}_k^- - \mathbf{K}_k \mathbf{P}_{z,k} \mathbf{K}_k^T$
End of interrupt routine

In summary, the EKF is suitable for systems with mild non-linearity, while the UKF is more robust and suitable for systems with strong non-linearity. The UKF introduces sigma points to not only directly reflect the system evolution but also comprehensively capture system characteristics. Therefore, when dealing with nonlinear systems, the UKF holds a distinct advantage over the EKF, allowing for more accurate estimation by better capturing the characteristics of system nonlinearities. Therefore, this work integrates the UKF to deal with the modeling nonlinearity in the industrial cooling fan and also proposes a state-dependent measurement covariance update mechanism to enhance the fan speed estimation online.

4 Industrial cooling fan speed estimation

The following simulation is conducted in MATLAB using the Runge–Kutta solver, with a numerical time step size set to 0.0005 s.

To apply the UKF algorithm to the cooling fan model, recall the cooling fan dynamic model in Eq. (9). Now, considering an external disturbance $\tau_d(t)$ and measurement noise $v(t)$, the model can be rewritten as

$$\dot{\omega}(t) = -a\omega(t) - a_N\omega^2(t) + b[\tau(t) + \tau_d(t)], \quad (25)$$

$$z(t) = \omega(t) + v(t), \quad (26)$$

where $\tau_d(t)$ and $v(t)$ are assumed to be Gaussian noise, with zero-mean and standard deviation σ_τ and σ_v, respectively.

$$\tau_d \sim \mathcal{N}(0, \sigma_\tau^2), \quad v \sim \mathcal{N}(0, \sigma_v^2). \quad (27)$$

To utilize the UKF, the forward difference method is applied to derive the discrete-time model

$$\dot{x}_k \approx \frac{x_{k+1} - x_k}{T}, \quad (28)$$

where T is the sample interval.

Based on Eq. (28), the discrete-time model can be written as

$$\omega_{k+1} = (1 - aT)\omega_k - a_N T\omega_k^2 + bT(\tau_k + \tau_{d,k}), \quad (29)$$

$$z_k = \omega_k + v_k. \quad (30)$$

The model for UKF can be constructed as follows:
(1) State transition equation:

$$\omega_{k+1} = (1 - aT)\omega_k - a_N T\omega_k^2 + bT\tau_k. \quad (31)$$

(2) Observation equation:

$$z_k = \omega_k. \quad (32)$$

(3) State and noise covariance:

$$\mathbf{x}_k = [\omega_k],$$
$$\mathbf{Q}_k = E\{\mathbf{w}_k\mathbf{w}_k^T\} = E\{b^2T^2\tau_{d,k}^2\} = b^2T^2\sigma_\tau^2, \quad (33)$$
$$\mathbf{R}_k = E\{\mathbf{v}_k\mathbf{v}_k^T\} = E\{v_k^2\} = \sigma_v^2.$$

For Eq. (33), the covariance matrices **Q** and **R** play a crucial role in affecting the performance and accuracy of the state estimation. **Q** represents the uncertainty in the system's process model. On the other hand, **R** represents the noise level in the measurements. The ratio between **Q** and **R** determines how much the filter relies on the model prediction *versus* the measurements.

For comparative analysis, the model for EKF is also derived as follows.
(4) The prior estimate:

$$\hat{\omega}_k^- = (1 - aT)\hat{\omega}_{k-1} - a_N T\hat{\omega}_{k-1}^2 + bT\tau_k. \quad (34)$$

(5) The Jacobians:

$$\mathbf{F}_k = \frac{\partial \mathbf{f}(\hat{\mathbf{x}}_{k-1})}{\partial \mathbf{x}} = (1 - aT) - 2a_N T\hat{\omega}_{k-1},$$
$$\mathbf{H}_k = \frac{\partial \mathbf{h}(\hat{\mathbf{x}}_k^-)}{\partial \mathbf{x}} = 1. \quad (35)$$

The input signal applies a stair-like excitation signal, as described in the study of Peng and Chen [13], and the sample interval T is 0.01 s. The cooling fan parameters are set as $J = 0.15$, $\alpha = 0.012$, and $C_D = 0.25$ (*i.e.*, $a = 0.08$, $a_N = 1.6667$, and $b = 6.6667$), of which the value of the lumped drag coefficient C_D is slightly larger to increase the nonlinearity in this model.

The system starts from rest, thus $\omega_0 = 0$, and both process and measurement noise are Gaussian white noise to verify the feasibility of the algorithms. The variance of external disturbance and measurement noise is set as $\sigma_\tau^2 = 2$ and $\sigma_v^2 = 2$. The covariances for UKF and EKF are set to $\mathbf{Q} = 1$ and $\mathbf{R} = 2$, respectively. For UKF, the relevant parameters for sigma point generation are empirically set as $\kappa = 10$, $\alpha = 0.25$, $\gamma = -0.3125$, and $\beta = 2$. The number of sigma points equals $2n + 1$, where n represents the system dimension [25].

To highlight the superiority of the UKF in estimating cooling fan system speed, the parameters of the nonlinear terms in the physical model were intentionally increased to emphasize the performance of both methods in state estimation under conditions where nonlinear effects are more pronounced. Figure 2 illustrates the speed estimation results using the EKF and UKF algorithms. As magnified in Figure 2 inset, taking a closer look at the transient response
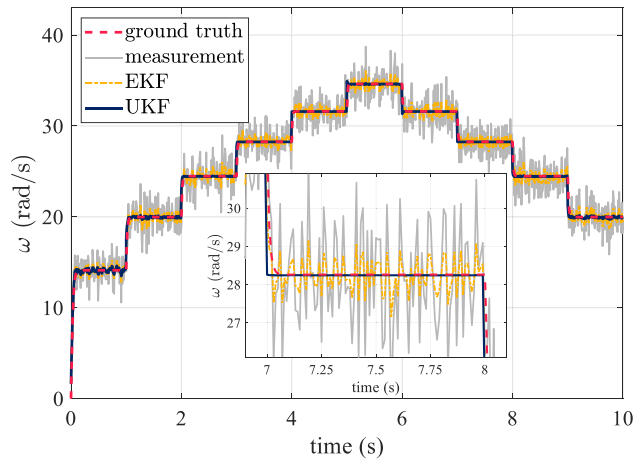
Figure 2: Comparison of speed estimates: EKF *vs* UKF, with partial enlargement (inset).

Figure 3: Comparison of the speed estimation error: EKF *vs* UKF.

as an example, one can observe that the EKF algorithm provides a relatively poor estimation, while the UKF yields a more precise speed estimate. In Figure 3, the estimation error between the results and the ground truth is further presented, with root-mean-square (RMS) errors of 0.5608 and 0.3661 for EKF and UKF, respectively. This clearly demonstrates that when the nonlinearity is significant, the local linearization of EKF fails to fully capture the system's nonlinear behavior, and the UKF exhibits superior state estimation ability in the presence of nonlinearities.

Figure 2 highlights the impressive estimation performance, achieved through meticulous adjustment of $\mathbf{Q}$ and $\mathbf{R}$ in UKF, when the system model has high nonlinearity. However, real-world scenarios introduce complexities, leading to the emergence of non-uniform Gaussian perturbations in the fan system. Factors such as modeling errors, inaccuracies in parameter identification, and parameters' slow time-varying property contribute to uncertainties in the fan system model. These uncertainties result in a non-Gaussian distribution of process noise, 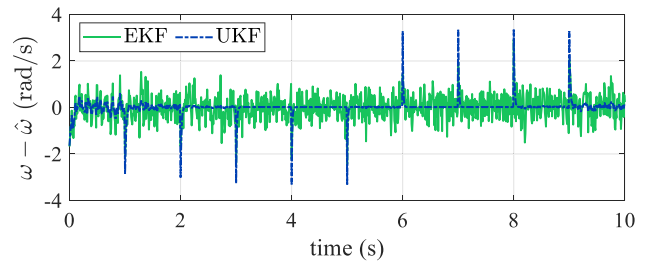causing estimation errors that deviate from a normal distribution and significantly impact the traditional UKF's performance.

To enhance the accuracy of fan speed estimation in the presence of non-uniform Gaussian perturbations, this article proposes strategic approaches. First, a modulation technique for the measurement noise covariance $\mathbf{R}$ of the UKF is introduced in this section, acknowledging the inconsistency of noise levels in practical scenarios. Second, a parameter update framework is presented, aiming to address prescribed errors in both parameter variations and modeling uncertainties.

The ensuing discussion will explore errors related to sensor noise, modeling, and parameter identification, offering valuable insights into strategies for setting $\mathbf{Q}$ and $\mathbf{R}$ within the specific context of fan speed estimation using the UKF.

4.1 Measurement noise modeling

In the previous sections, the observation disturbance is assumed to be homoscedastic, that is, the variance remains constant throughout the rotation speed, as shown in Figure 4(a). However, based on the practical experiment observations, it is revealed that the amount of noise becomes larger with a higher fan speed. In this case, the noise of the cooling fan should be assumed to be heteroscedastic, which means that the variance depends on the value of the speed. Figure 4(b) demonstrates that as the value becomes larger, the data points are more widely
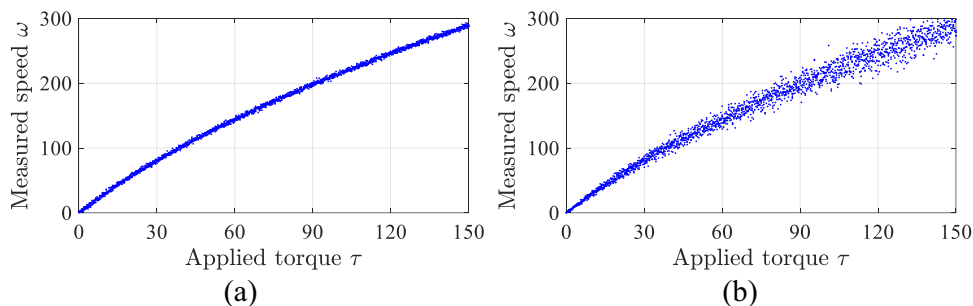

Figure 4: Noise behavior statistical analysis. (a) Homoscedasticity. (b) Heteroscedasticity.

distributed due to its larger variance, showing the heteroscedasticity of the noise.

Assume that the standard deviation is a function of speed

$$\sigma_k(\omega_k, \mathbf{a}) = a_1\omega_k + a_2, \tag{36}$$

where $\mathbf{a} = [a_1 \ a_2]^T$ are the parameters to be determined, and σ_k is the standard deviation at time step k.

The fitting problem is fitted into

$$\arg\min_{\mathbf{a}} f(\mathbf{a}) = \arg\min_{\mathbf{a}} (\sigma_k - \hat{\sigma}_k(\omega_k, \mathbf{a}))^2. \tag{37}$$

Monitoring different values of the fan speed, collecting the measured data, and calculating the standard deviations yield

$$\begin{bmatrix} \sigma_1 \\ \vdots \\ \sigma_k \end{bmatrix} = \begin{bmatrix} \omega_1 & 1 \\ \vdots & \vdots \\ \omega_k & 1 \end{bmatrix}\begin{bmatrix} a_1 \\ a_2 \end{bmatrix}. \tag{38}$$

The parameter vector $\mathbf{a}$ can be solved using the well-known least-squares solution. Finally, the modulation of $\mathbf{R}$ can be established by

$$\mathbf{R}_k = \hat{\sigma}_k^2(\omega_k, \mathbf{a}), \tag{39}$$

with a time-varying noise covariance $\mathbf{R}_k$; the degree of belief in measurements can be adjusted and give a better approximation.

4.2 Cooling fan modeling error discussion

In a recent study on the estimation of cooling fan parameters [13], the real-time parameter estimation results show that for every stair change in the given input, the estimated values exhibit sharp fluctuations, which mainly results from the error of modeling. Recalling the cooling fan model Eq. (9), the transient response of the electrical dynamics is neglected since its time constant L/R is much smaller in magnitude than the mechanical time constant J_m/B_m. If the electrical dynamics is reconsidered, the overall real system can be described as a second-order system:

$$L\frac{di(t)}{dt} + Ri(t) + K\omega(t) = V_{in}(t), \tag{40}$$

$$J_m\frac{d\omega(t)}{dt} = -B_m\omega(t) - C_d\omega^2(t) + Ki(t). \tag{41}$$

The system in Eqs. (40) and (41) become relatively complex and, unfortunately, the information of current i is not available for general industrial cooling fan systems. Thus, parameter identification for Eq. (40) cannot be conducted.

As a result, the second-order system is reduced by a first-order nonlinear dynamic equation, where the equivalent equation is expressed as Eq. (7). Note that the equivalent parameters Eq. (8) are based on the fact that the driver dynamics is completely ignored. The model reduction process is described in Section 2.

Since only the fan speed output is available, this work attempts to use Figure 5(b) to replace Figure 5(a) as a reduced-order model for equivalent parameter identification. Note that the equivalent first-order model reduction assumes that the electrical dynamics is much faster than the mechanical fan dynamics. This assumption is reasonable and is going to be illustrated by the following simulation and experimental comparison.

To demonstrate the model mismatch behavior caused by the electrical dynamics, $L = 0.01$, $R = 1$, $K = 1$, $J_m = 0.15$, $B_m = 0.012$, and $C_d = 0.0025$. Based on the output speed, Eq. (7) was further considered to approximate the responses Eqs. (40) and (41), the associated estimated equivalent parameters are $J = 0.1635$, $\alpha = 1.0106$, and $C_D = 0.0025$, respectively. The corresponding simulation is shown in Figure 6(a).

Based on the given stair-liked excitation input signal, the simulation results considering Eqs. (40) and (41) show that for an abrupt change in the applied input, the speed response possesses a relatively smooth rising speed within a short period of time. However, the simulation result using Eq. (7) illustrates a sharp rising speed. This slight difference comes from the model reduction or the so-called modeling errors. The qualitative behavior can also be observed from the experiment, as illustrated in Figure 6(b), which further validates the assumption. Consequently, the mismatches between the real system and the equivalent system leads to fluctuation of estimates whenever the applied input changes abruptly.

In conclusion, the main reason this work considered a model reduction is that the current output, generated from Eq. (40), for the general industrial fans in the market is not available. To avoid the use of the current information for cooling fan modeling and fan speed prediction, this work
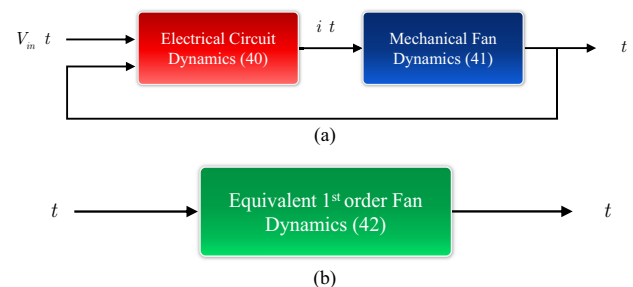
Figure 5: Cooling fan system representation and model reduction. (a) Electrical-circuit-derived second-order fan dynamics. (b) First-order equivalent cooling fan model reduction equivalent representation.

applied a modeling reduction. Figure 6(a) and (b) verify the reasonability of this consideration.

To address this issue and further amend the estimated biases identified in the UKF, the parameter update method with UKF is introduced to refine the speed estimates and to pursue unbiased estimates, and the equivalent system Eq. (7) and the proposed parameter update mechanism are used to make up for the model discrepancy and the parameter identification error.

4.3 UKF with parameter update mechanism

Recalling the cooling fan model in Eqs. (25) and (26), through diverse scenarios encompassing different environments, time frames, and operational conditions, it has been observed from experience that the model parameters of the fan system may undergo slight perturbations, suggesting the potential for time-varying characteristics.

Consequently, we attribute the effects of model uncertainty or disturbances in the fan to the variation of system parameters. Based on this assumption, an online parameter estimation mechanism to enhance unbiased estimation of fan speed is conducted.

Consider the formulation of these time-varying parameters as follows.

$$
\begin{aligned}
a(t) &= \hat{a} + \tilde{a}(t), \\
a_N(t) &= \hat{a}_N + \tilde{a}_N(t), \\
b(t) &= \hat{b} + \tilde{b}(t),
\end{aligned}
\tag{42}
$$

where $\hat{a}$, $\hat{a}_N$, and $\hat{b}$ are the estimated values obtained from the identification results by the low-pass filtering method [13] and $\tilde{a}(t)$, $\tilde{a}_N(t)$, and $\tilde{b}(t)$ are the time-varying parameter uncertainties, describing the effects of the modeling errors and external perturbations. The main strategy in this section is to consider the parameter uncertainties as variables, whose change rates $\dot{\tilde{a}}$, $\dot{\tilde{a}}_N$, and $\dot{\tilde{b}}$ are assumed to be Gaussian distributions with zero means and standard deviations σ_a, σ_{a_N}, and σ_b, respectively. That is, the dynamics of the parameter uncertainties satisfy

$$
\begin{aligned}
\dot{\tilde{a}} &= w_a, \quad w_a \sim \mathcal{N}(0, \sigma_a^2), \\
\dot{\tilde{a}}_N &= w_{a_N}, \quad w_{a_N} \sim \mathcal{N}(0, \sigma_{a_N}^2), \\
\dot{\tilde{b}} &= w_b, \quad w_b \sim \mathcal{N}(0, \sigma_b^2).
\end{aligned}
\tag{43}
$$

Thus, the overall system can be described as follows:
(1) Process model:

$$
\begin{aligned}
\dot{\omega}(t) &= -[\hat{a} + \tilde{a}(t)]\omega(t) - [\hat{a}_N + \tilde{a}_N(t)]\omega^2(t) \\
&\quad + [\hat{b} + \tilde{b}(t)][\tau(t) + \tau_d(t)], \\
\dot{\tilde{a}}(t) &= w_a(t), \\
\dot{\tilde{a}}_N(t) &= w_{a_N}(t), \\
\dot{\tilde{b}}(t) &= w_b(t).
\end{aligned}
\tag{44}
$$

(2) Observation equation:

$$
z(t) = \omega(t) + v(t),
\tag{45}
$$

of which ω, $\tilde{a}$, $\tilde{a}_N$, and $\tilde{b}$ are the states of the system, and τ_d, w_a, w_{a_N}, and w_b are the perturbations.

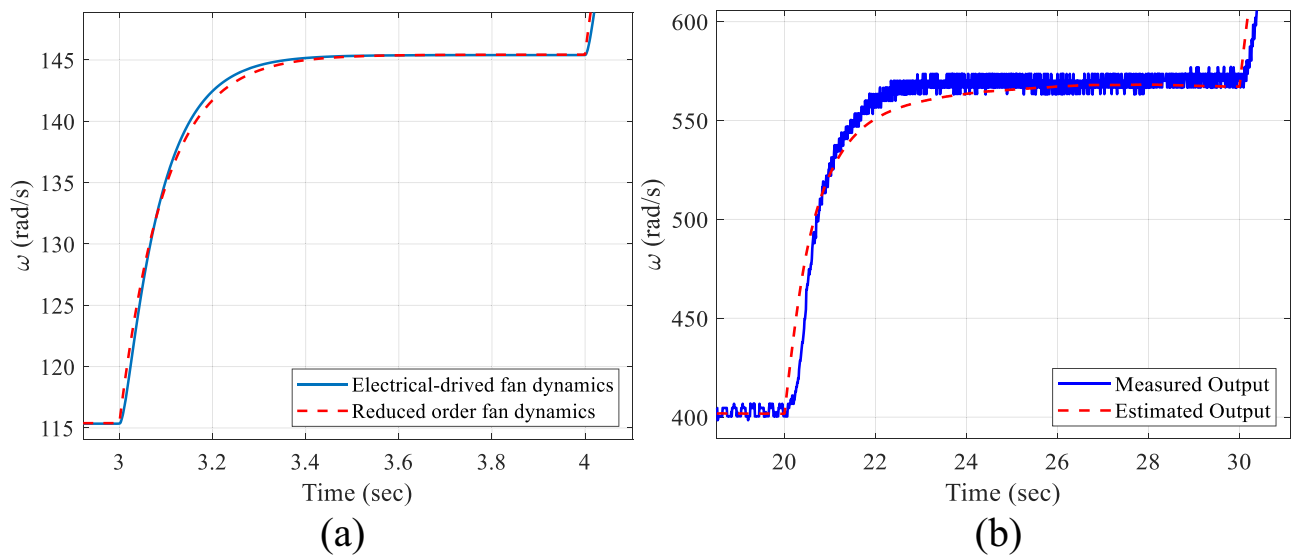Similarly, to utilize the UKF algorithm, the discrete-

Figure 6: Cooling fan system transient speed response comparison between the electrical-circuit-derived second-order fan dynamics and the reduced order cooling fan representation. (a) Simulation observation. (b) Experimental validation.

time model representation of Eq. (44) is derived through the forward difference, given by

$$\omega_{k+1} = [1 - (\hat{a} + \tilde{a}_k)T]\omega_k - (\hat{a}_N + \tilde{a}_{N,k})T\omega_k^2$$
$$+ (\hat{b} + \tilde{b}_k)T(\tau_k + \tau_{d,k})$$
$$\tilde{a}_{k+1} = \tilde{a}_k + Tw_{a,k} \qquad (46)$$
$$\tilde{a}_{N,k+1} = \tilde{a}_{N,k} + Tw_{a_N,k}$$
$$\tilde{b}_{k+1} = \tilde{b}_k + Tw_{b,k},$$

and

$$z_k = \omega_k + v_k. \qquad (47)$$

Concerning the discrete-time model Eq. (46), the actual change rates of uncertainties are unknown in the real world. Fortunately, based on practical experimental statistics, parameter uncertainties can be assumed to be slowly time-varying. Therefore, the practical framework of the UKF for online realization can be modeled as the following transition equation.

(3) State transition equation:

$$\omega_{k+1} = [1 - (\hat{a} + \tilde{a}_k)T]\omega_k - (\hat{a}_N + \tilde{a}_{N,k})T\omega_k^2$$
$$+ (\hat{b} + \tilde{b}_k)T\tau_k,$$
$$\tilde{a}_{k+1} = \tilde{a}_k, \qquad (48)$$
$$\tilde{a}_{N,k+1} = \tilde{a}_{N,k},$$
$$\tilde{b}_{k+1} = \tilde{b}_k,$$

where the initial condition of the parameters can be obtained from the estimation algorithms [13,14].

(4) Observation equation:

$$z_k = \omega_k. \qquad (49)$$

(5) The state vector, the process, and measurement noise are expressed as follows:

$$\mathbf{x}_k = \begin{bmatrix} \omega_k \\ \tilde{a}_k \\ \tilde{a}_{N,k} \\ \tilde{b}_k \end{bmatrix}, \quad \mathbf{w}_k = \begin{bmatrix} (\hat{b} + \tilde{b}_k)T\tau_{d,k} \\ Tw_{a,k} \\ Tw_{a_N,k} \\ Tw_{b,k} \end{bmatrix}, \quad \mathbf{v}_k = [v_k], \quad (50)$$

and

$$\mathbf{Q}_k = E\{\mathbf{w}_k\mathbf{w}_k^T\}$$
$$= \begin{bmatrix} (\hat{b} + \tilde{b}_k)^2 T^2 \sigma_\tau^2 & 0 & 0 & 0 \\ 0 & T^2\sigma_a^2 & 0 & 0 \\ 0 & 0 & T^2\sigma_{a_N}^2 & 0 \\ 0 & 0 & 0 & T^2\sigma_b^2 \end{bmatrix}, \qquad (51)$$
$$\mathbf{R}_k = E\{\mathbf{v}_k\mathbf{v}_k^T\} = \sigma_{v,k}^2(\omega, \hat{\mathbf{a}}).$$

Note that $\tau_{d,k}$, $w_{a,k}$, $w_{a_N,k}$, and $w_{b,k}$ are assumed to be statistically independent.

The simulation condition is mainly given the same as in the previous instance, where the simulation signal is obtained by the nominal parameters given by $J = 0.15$, $\alpha = 0.012$, and $C_D = 0.0025$ (*i.e.* $a = 0.08$, $a_N = 0.0167$, and $b = 6.6667$). Based on the studies of Chen and Peng, Li *et al.*, and Peng *et al.* [32–34], the parameters utilized in UKF are assumed to have 10% uncertainty. That is, $\hat{a} = 0.9a$, $\hat{a}_N = 0.9a_N$, and $\hat{b} = 0.9b$, and their variances $\sigma_a^2 = 0.1a$, $\sigma_{a_N}^2 = 0.1a_N$, and $\sigma_b^2 = 0.1b$ are applied to construct $\mathbf{Q}_k$ in Eq. (51). For the comparison of estimation performance, the covariance values for the standard UKF are set to $\mathbf{Q} = 2$ and $\mathbf{R} = 2$.

Figure 7 shows the speed estimating results for the general UKF and the proposed method, which evidently shows that with the parameter update mechanism, the biased estimate issue from the parameter uncertainty is eliminated, and the effect of noise is attenuated as well. Figure 8 provides the numerical errors between the estimation results and the ground truth. One can observe that the error of the traditional UKF is not zero-mean and is noisier, while the proposed mechanism alleviates the bias phenomenon and efficiently filters out the noise. The RMS errors are quantified as 1.3393 for the traditional UKF and significantly reduced to 0.7485 for the UKF with the parameter update mechanism.

Based on simulation results, the conclusion is drawn that under the influence of time-varying uncertainties in perturbation, the traditional UKF, while adjustable through tuning $\mathbf{Q}$ to modify estimation performance, still exhibits inherent biases in state estimation regardless of the adjustments made. In comparison, the UKF with a parameter update mechanism offers a more versatile solution, preventing biases in state
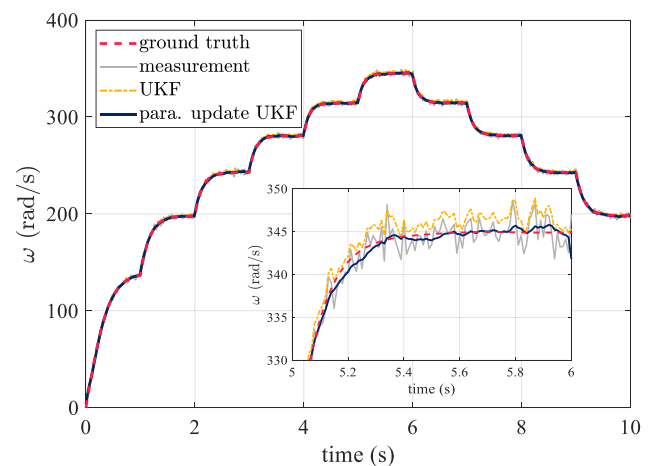

Figure 7: Speed estimate by UKF with the parameter update mechanism.
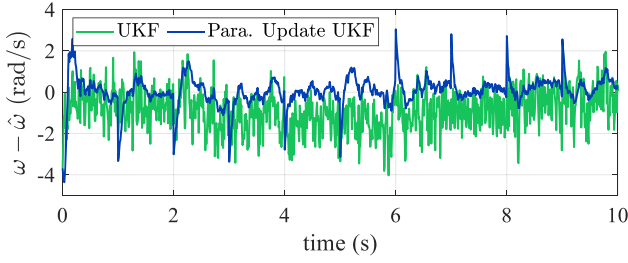
Figure 8: Speed estimation error by UKF with the parameter update mechanism.

estimation and effectively reducing the interference of measurement noise.

5 Experimental validation

To examine the feasibility of the proposed methods, the algorithms are implemented in an embedded platform for validation. The module of the multi-fan embedded platform is illustrated in Figure 9. The printed circuit board connects the microprocessor Teensy 3.6 with other components, as shown in Figure 9(b) and (c). These components include eight industrial cooling fans, eight knobs for users to manually set the desired speed or control inputs for each fan, eight LEDs indicating the status of each fan, an OLED display showing detailed system information, and two buttons that switch the experiments to different modes. An USB port allows for communication between the PC and Teensy 3.6, which is also the power supplier for the microprocessor.

System identification is realized through the application of the low-pass filtering method, as established in the recent research [13]. The equivalent model parameters in Eq. (7) are identified as $J = 0.4083$, $\alpha = 0.3151$, and $C_D = 7.02 \times 10^{-4}$.

5.1 Experiments on R modulation

In preparation for applying UKF algorithms to the cooling fans, the modulation of the covariance **R** must be carried out first. As hypothesized, the variance **R** is a function of fan speed as described by Eq. (39). To determine the relationship between **R** and the speed, a series of different speed values should be collected, then the standard deviations at different speed levels can be calculated. However, the data collection is memory-requested. Aiming at this issue, the recursive mean and recursive standard deviation are applied [35].
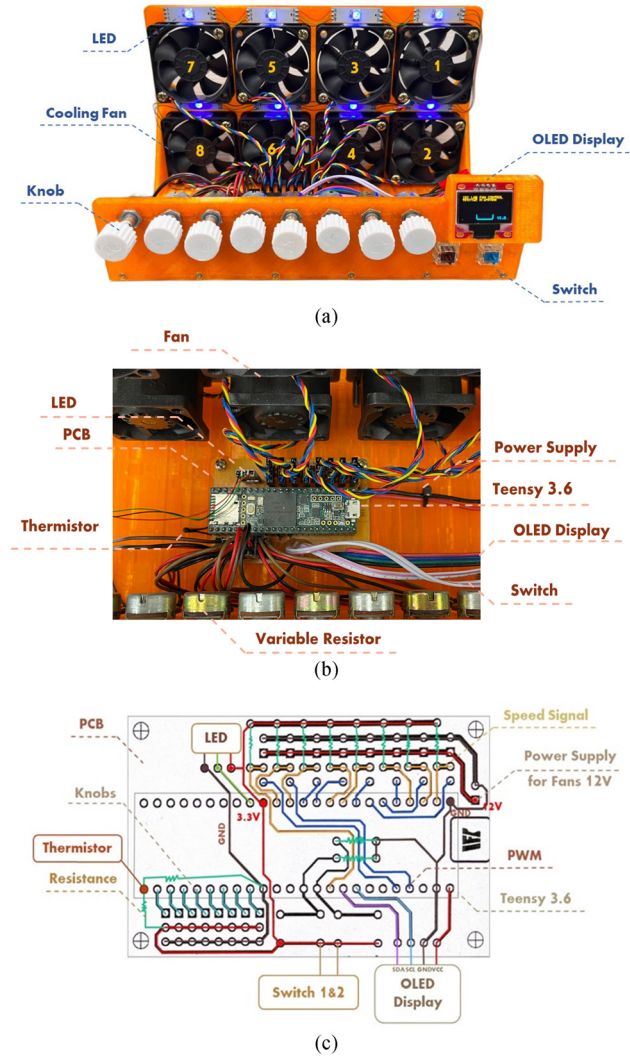

Figure 9: Prototype of the developed cooling fan tray system. (a) Front view of the fan tray system. (b) Microprocessor used for the proposed algorithm realization. (c) PCB layout.

$$\mu_k = \frac{k-1}{k}\mu_{k-1} + \frac{1}{k}\omega_k, \tag{52}$$

$$\mathrm{Var}_k = \frac{k-1}{k}\mathrm{Var}_{k-1} + \frac{1}{k}(\omega_k - \mu_k)^2 + \frac{k-1}{k}(\mu_{k-1} - \mu_k)^2, \tag{53}$$

then $\sigma_k = \sqrt{\mathrm{Var}_k}$.

Applying a fixed step input, the speed will reach a steady state after 3 s, and the recursions start at this point. The embedded system only needs to store the final value of the recursion and repeat this process for several different levels of fixed input voltages. The relationship between **R** and the speed can therefore be obtained by Eq. (38) using a considerably smaller memory size. Figure 10 demonstrates
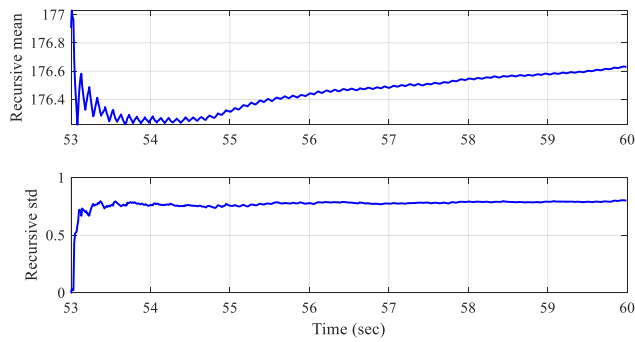
Figure 10: Recursive mean and recursive standard deviation.

Table 1: Statistical data of fan 1

PWM (%)	Speed (rps)	Std.	Variance R
9.9992	13.4706	0.0514	0.0026
23.3326	38.9528	0.1599	0.0255
36.6659	78.5468	0.3203	0.1026
49.9992	110.2039	0.3951	0.1561
63.3326	137.4071	0.5812	0.3377
76.6659	163.9589	0.6823	0.4656
89.9992	189.3101	0.7070	0.4998

the recursion process at PWM = 80%, and the overall statistical data are recorded in Table 1.

Based on the assumption of heteroscedasticity and the prescribed formulation, the parameters describing the relationship between the speed and standard deviation can be derived by the least-squares solution, as shown in Figure 11.

5.2 Experiments on UKF with parameter update mechanism

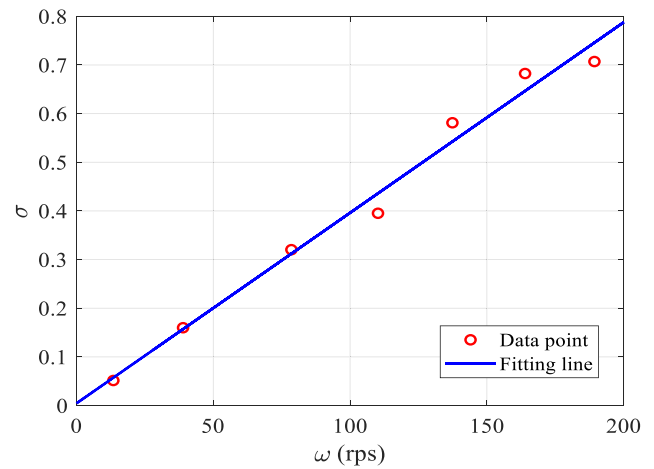The experiments on speed estimation were conducted using two input scenarios: (i) a stair input PWM (Figure 12)

Figure 11: Fitting line for speed and standard deviation of fan 1 with $a_1 = 0.0039$ and $a_2 = 0.0045$.

and (ii) manual modulation using knob 1 (Figures 13 and 14). In the case of the traditional UKF, a tradeoff arises where a smoother speed requires higher confidence in the mathematical model. However, inherent model and parameter uncertainties in the system lead to a biased speed estimate, as depicted in Figure 12(b) and (c). Conversely, prioritizing an unbiased estimate places greater emphasis on trusting the measurements, which can lead to a decrease in filter effectiveness. As seen in Figure 13(b), the traditional UKF estimate (red line) closely aligns with the measured value (gray line).

In contrast, the proposed UKF with a parameter update mechanism demonstrates the ability to achieve an unbiased estimate while simultaneously filtering out undesirable noise for both types of input PWM. Figure 13(c) illustrates the corresponding speed estimation errors. Furthermore, Figures 12(c) and 13(c) highlight the proposed method's capability to mitigate modeling errors that arise from neglecting the electrical driver model. A comparative analysis between Figures 12(b) and 13(b) leads to the conclusion that, for the traditional UKF, the adjustment of **Q** and **R** can be a cumbersome process. An undersized
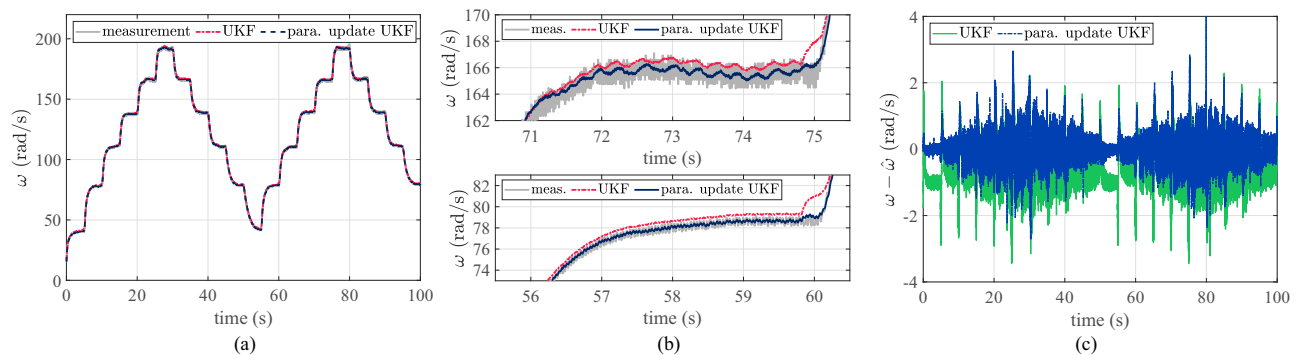

Figure 12: Speed estimates by UKF and UKF with parameter update for stair input. (a) Speed estimation comparison. (b) Responses – partial enlargement. (c) Speed estimation errors.
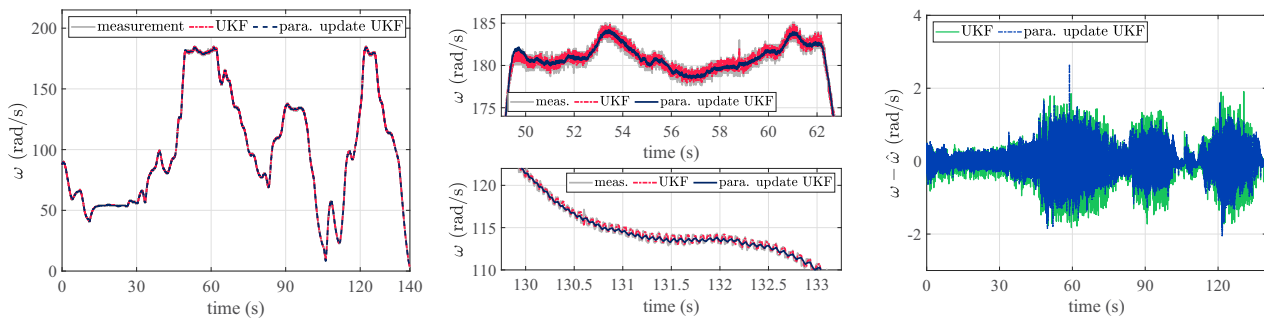
Figure 13: Speed estimates by UKF and UKF with parameter update for manual modulation input. (a) Speed estimation comparison. (b) Responses – partial enlargement. (c) Speed estimation errors.
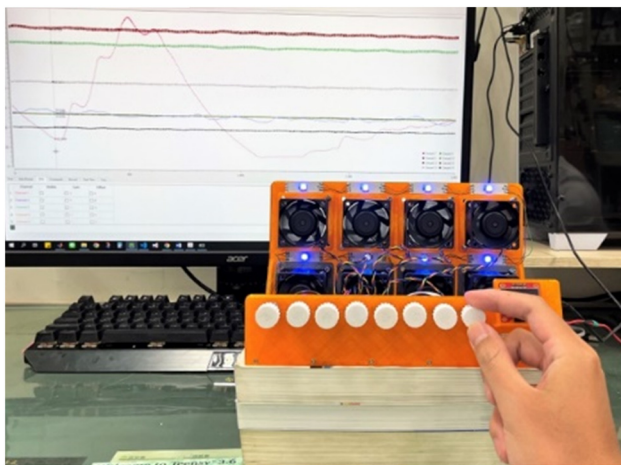

Figure 14: Manual modulation of fan input commands.

$\mathbf{Q}$ and $\mathbf{R}$ ratio results in biased estimation states, while an oversized $\mathbf{Q}$ and $\mathbf{R}$ ratio causes the estimated states to resemble noisy signals. In contrast, the proposed UKF with a parameter update mechanism adeptly avoids such issues.

6 Conclusions

This article conducts a detailed case study on real-time speed estimation for cooling fan arrays in source-limited embedded systems, considering modeling uncertainties and the presence of measurement noise. With a focus on practical applications in fan systems, the study proposes a set of strategies to enhance fan speed estimation using the UKF state estimation technique. The discussion encompasses the effect of model reduction, nonlinear model speed estimation, characteristics of speed measurement noise, and the time-varying parameter-dependent uncertainties in fan system models. To address noise during fan measurements, the study utilizes noise modeling to enable automatic modulation of the covariance $\mathbf{R}$ related to speed. Concurrently, the study conducts a thorough analysis of the impact of modeling errors in fan systems and the non-uniform Gaussian disturbances caused by parameter identification errors. The article concludes by introducing a UKF with a parameter update mechanism for fan speed estimation, validated through simulations and experiments to showcase the method's effectiveness. The proposed UKF framework with a parameter update mechanism exhibits outstanding performance in real-world fan speed estimation applications, demonstrating superior estimation accuracy compared to the traditional UKF. The estimated states effectively achieve a balanced representation of the model and measurement values. Moreover, the estimated speeds are much smoother than the raw measurements. From the control point of view, the fused speed can avoid serious control chattering and thereby the proposed method can further attenuate control energy loss.

Author contributions: Conceptualization, C. C. Peng; methodology, C. C. Peng; software, M. C. Tsai and T. Y. Chen; validation, M. C. Tsai and T. Y. Chen; formal analysis, C. C. Peng and M. C. Tsai; investigation, C. C. Peng, M. C. Tsai and T. Y. Chen; resources, C. C. Peng; data curation, T. Y. Chen; writing – original draft preparation, M. C. Tsai and T. Y. Chen; writing – review and editing, C. C. Peng; visualization, M. C. Tsai; supervision, C. C. Peng; project administration, C. C. Peng; funding acquisition, C. C. Peng. All authors have accepted responsibility for the entire content of this manuscript and consented to its submission to the journal,

reviewed all the results and approved the final version of the manuscript.

Conflict of interest: The authors declare no conflicts of interest.

Data availability statement: The data that support the findings of this study are available from the corresponding author, C.C. Peng, upon reasonable request.

References

[1] Li C, Li J. Passive cooling solutions for high power server CPUs with pulsating heat pipe technology. Front Energy Res. 2021;9:755019.

[2] Wang Z, Bash C, Tolia N, Marwah M, Zhu X, Ranganathan P. Optimal fan speed control for thermal management of servers. ASME 2009 InterPACK Conference. Vol. 22009, 2009. p. 709–19.

[3] Peng CC, Lin YI, eds. Dynamics modeling and parameter identification of a cooling fan system. 2018 IEEE International Conference on Advanced Manufacturing (ICAM); 2018.

[4] Staats WL. Active heat transfer enhancement in integrated fan heat sinks [doctoral dissertation]. Cambridge, Massachusetts, USA: Massachusetts Institute of Technology; 2012.

[5] Yoon Y, Kim DR, Lee K-S. Cooling performance and space efficiency improvement based on heat sink arrangement for power conversion electronics. Appl Therm Eng. 2020;164:114458.

[6] Jian-Hui Z, Chun-Xin Y. Design and simulation of the CPU fan and heat sinks. IEEE Trans CompPackaging Technol. 2008;31(4):890–903.

[7] Huang J, Naini SS, Miller R, Rizzo D, Sebeck K, Shurin S, et al. A hybrid electric vehicle motor cooling system – design, model, and control. IEEE Trans Veh Technol. 2019;68(5):4467–78.

[8] Kheirabadi AC, Groulx D. Cooling of server electronics: A design review of existing technology. Appl Therm Eng. 2016;105:622–38.

[9] Xijin T, ed. Cooling fan reliability: failure criteria, accelerated life testing, modeling and qualification. RAMS '06 Annual Reliability and Maintainability Symposium, 2006; 2006.

[10] Afshar M, Li C, Akin B. Real-time current-based distributed bearing faults detection in small cooling fan motors. IEEE Trans Ind Appl. 2024;60(2):3188–99.

[11] Jin X, Ma EWM, Cheng LL, Pecht M. Health monitoring of cooling fans based on Mahalanobis distance with mRMR feature selection. IEEE Trans Instrum Meas. 2012;61(8):2222–9.

[12] Peng C-C, Chen Y-H. A hybrid neural ordinary differential equation based digital twin modeling and online diagnosis for an industrial cooling fan. Future Internet. 2023;15(9):302.

[13] Peng C-C, Chen T-Y. A recursive low-pass filtering method for a commercial cooling fan tray parameter online estimation with measurement noise. Measurement. 2022;205:112193.

[14] Peng CC, Su CY. Modeling and parameter identification of a cooling fan for online monitoring. IEEE Trans Instrum Meas. 2021;70:1–14.

[15] Gong X, Qiao W. Current-based mechanical fault detection for direct-drive wind turbines via synchronous sampling and impulse detection. IEEE Trans Ind Electron. 2015;62(3):1693–702.

[16] Wang XB, Yang ZX, Yan XA. Novel particle swarm optimization-based variational mode decomposition method for the fault diagnosis of complex rotating machinery. IEEE/ASME Trans Mechatron. 2018;23(1):68–79.

[17] Welch G, Bishop G. An introduction to the Kalman filter. Chapel Hill, United States: University of North Carolina; 1995.

[18] Zhanlue Z, Huimin C, Genshe C, Chiman K, Li XR, eds. Comparison of several ballistic target tracking filters. 2006 American Control Conference; 2006.

[19] Lee JH, Ricker NL, eds. Extended Kalman filter based nonlinear model predictive control. 1993 American Control Conference; 1993.

[20] Ribeiro MI. Kalman and extended kalman filters: Concept, derivation and properties. Inst Syst Robot. 2004;43(46):3736–41.

[21] Wan EA, Merwe RVD, eds. The unscented Kalman filter for nonlinear estimation. Proceedings of the IEEE 2000 Adaptive Systems for Signal Processing, Communications, and Control Symposium (Cat No00EX373); 2000.

[22] Kandepu R, Foss B, Imsland L. Applying the unscented Kalman filter for nonlinear state estimation. J Process Control. 2008;18(7):753–68.

[23] Kwok NM, Gu F, Zhou W, eds. Evolutionary particle filter: re-sampling from the genetic algorithm perspective. 2005 IEEE/RSJ International Conference on Intelligent Robots and Systems; 2005.

[24] Wigren A, Murray L, Lindsten F. Improving the particle filter in high dimensions using conjugate artificial process noise. IFAC-PapersOnLine. 2018;51(15):670–5.

[25] Julier SJ, Uhlmann JK, eds. New extension of the Kalman filter to nonlinear systems. Signal processing, sensor fusion, and target recognition VI. Spie. Conference paper presented at 'Signal Processing, Sensor Fusion, and Target Recognition VI,' Vol. 3068, Orlando, FL, United States; 1997.

[26] Julier SJ, Uhlmann JK. Unscented filtering and nonlinear estimation. Proc IEEE. 2004;92(3):401–22.

[27] Lyu X, Hu B, Li K, Chang L. An adaptive and robust UKF approach based on Gaussian process regression-aided variational Bayesian. IEEE Sens J. 2021;21(7):9500–14.

[28] Zhu F, Fu J. A novel state-of-health estimation for Lithium-Ion battery via unscented Kalman filter and improved unscented particle filter. IEEE Sens J. 2021;21(22):25449–56.

[29] Tan B, Zhao J, Terzija V, Zhang Y. Decentralized data-driven estimation of generator rotor speed and inertia constant based on adaptive unscented Kalman filter. Int J Electr Power Energy Syst. 2022;137:107853.

[30] Lv X, Zhang Y, eds. Extended Kalman filter infusion algorithm design and application characteristics analysis to stochastic closed loop fan speed control of the nonlinear turbo-fan engine. Singapore: Springer Singapore; 2019.

[31] Gong CSA, Lee HC, Chuang YC, Li TH, Su CHS, Huang LH, et al. Design and implementation of acoustic sensing system for online early fault detection in industrial fans. J Sens. 2018;2018:4105208.

[32] Chen L-H, Peng C-C. Extended backstepping sliding controller design for chattering attenuation and its application for servo motor control. Appl Sci. 2017;7(3):220.

[33] Li Y-R, Peng C-C, Juang J-N. An integral method for parameter identification of a nonlinear robot subject to quantization error. Nonlinear Dyn. 2023;111(24):22419–41.

[34] Peng C-C, Cheng N-J, Tsai M-C. Application of an output filtering method for an unstable wheel-driven pendulum system parameter identification. Electronics. 2023;12(22):4569.

[35] Peng CC. Low-cost embedded real-time handheld vibration smart sensor for industrial equipment onsite defect detection. IEEE Open J Ind Electron Soc. 2021;2:469–78.